CRYSTAL GROWTH & DESIGN

Article

Cite This: Cryst. Growth Des. 2018, 18, 210−218

pubs.acs.org/crystal

Rapid Continuous Antisolvent Crystallization of Multicomponent Systems

Syed A. Raza,[†] Ulrich Schacht,[‡,∥] Vaclav Svoboda,[‡,∥] Darren P. Edwards,[†] Alastair J. Florence,[*,†,∥] Colin R. Pulham,[§] Jan Sefcik,[*,‡,∥] and Iain D. H. Oswald[*,†]

[†]Strathclyde Institute of Pharmacy and Biomedical Sciences (SIPBS), University of Strathclyde, 161 Cathedral Street, Glasgow, U.K. G4 0RE

[‡]Department of Chemical and Process Engineering, University of Strathclyde, 75 Montrose Street, Glasgow, U.K. G1 1XJ

[§]EaStCHEM School of Chemistry, University of Edinburgh, Joseph Black Building, David Brewster Road, Edinburgh, EH9 3FJ, U.K.

[∥]EPSRC Centre for Innovative Manufacturing in Continuous Manufacturing and Crystallisation, University of Strathclyde, Technology and Innovation Centre, 99 George Street, G1 1RD Glasgow, U.K.

Supporting Information

ABSTRACT: This paper describes the application of a novel antisolvent crystallization approach to rapid production of tunable solid solutions of hydrophobic amino acids, comprising L-leucine, L-isoleucine, and L-valine. The antisolvent approach provides an alternative to other crystallization routes, e.g., ball-milling, liquid-assisted grinding, and slurry methods, to achieve the required multicomponent solid phases. We report new crystal structures of L-leucine/L-isoleucine and L-leucine/L-valine, and confirm a recent report on a new form of L-isoleucine/L-valine. We used these multicomponent complexes as a test set of materials to demonstrate translation of small scale batch antisolvent crystallization to a continuous production process.

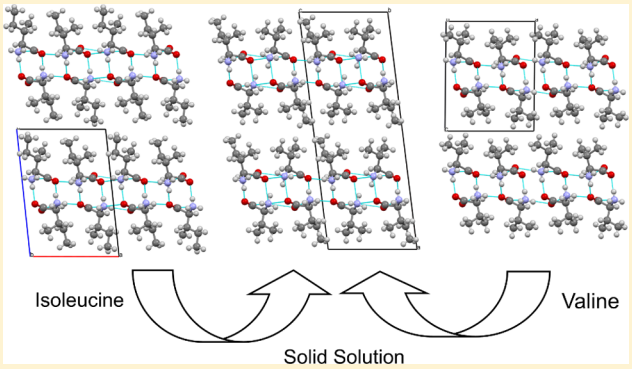

INTRODUCTION

Multicomponent complexes (MCCs) are materials that have two or more different molecules in the same crystal lattice.[1,2] MCCs can be classified into many different subsets that include cocrystals, solvates, and solid solutions. The interest in MCCs recently led to cocrystals being classified by the U.S. Food and Drug Administration for the first time to clarify their legal status.[3,4] Initially cocrystals were classified as "cocrystal drug product intermediates" rather than new active pharmaceutical ingredients (APIs); however they have recently been reclassified as a special case of a solvated product where the second component is nonvolatile.[5] MCCs in their various forms are products of crystal engineering, an area of science that has opened up the opportunity to design and tune the properties of materials such as luminescence,[6,7] detonation velocity,[8] bioavailability,[9] stability,[10,11] phase transition temperatures,[12] and processability.[13] The manipulation of hydrogen bonding and other intermolecular interactions to modify packing and create new materials without altering the covalent chemistry is a simple route to improve physical properties; e.g., larger insoluble medicinal products can be engineered to have better solubility characteristics.[14]

The development of industrial production of MCCs is challenging due to many problems and pitfalls related to scaling up their preparation. Even large scale crystallization of single component systems can give rise to problems of physical purity such as polymorphs, solvates, hydrates, and even amorphous content, and these can be exacerbated, for multicomponent systems, by the potential for crystals to have a varying composition, such as 1:1 or 2:1 cocrystals or solid solutions, giving rise to mixed phases. Many general crystallization methods that are successful for discovery at laboratory scale, such as solvent evaporation or antisolvent vapor diffusion, are not seen as a viable solution for the large scale crystallization process. Slurry-based methods are industrially feasible but suffer from the fact that they are usually nonstoichiometric and noncontinuous,[15,16] which leads to difficulties with reproducibility of particle size distribution and solid phase control. Supercritical fluid and twin-screw extrusion are other methods for industrial scale production of multicomponent systems which are reported as viable.[17−19] Previous work by Zhao et al. on cooling crystallization of a nutraceutical cocrystal has shown that continuous crystallization in an oscillatory baffled reactor offers potential benefits in terms of simplifying the scale-up and reducing the time scales of process development from starting materials to end product while retaining fine control of the

Received: August 8, 2017
Revised: November 6, 2017
Published: November 27, 2017

DOI: 10.1021/acs.cgd.7b01105
Cryst. Growth Des. 2018, 18, 210−218

product quality.[20] We have recently reported continuous crystallization of 1:1 and 2:1 cocrystals of benzoic acid and isonicotinamide via mixing-induced supersaturation using a concentric capillary mixer.[21] A key advantage is that continuous processes operate at steady state which ensures consistency of the final product in terms of crystalline form and particle size distribution and morphology.

Amino acids are crucial for maintenance of health and are used extensively in foods, supplements, and medicines, and as such their solid-state properties and structures have been thoroughly investigated under a range of conditions.[22−28] Very few studies have investigated the amino acids in terms of the production of MCCs and fully characterized the solid forms despite the importance of these materials. A search of the Cambridge Structural Database[29] has shown that typically structural studies have been limited to the crystallization of D- and L-enantiomers together, a view supported by a recent review of crystal structures of amino acids by Gorbitz.[30] The relatively low number of observations of structurally characterized amino acid MMCs has largely been attributed to the inefficient packing that would result if single enantiomer systems were crystallized together.[31−38] However, there have been a number of papers that have shown solid solutions exist. For example, Kamei et al. investigated the solid−liquid equilibria in L-isoleucine with L-alanine[39] and L-norleucine[40] and discovered that solid solutions of the systems exist through the identification of changes to the *c*-axis length on substitution of norleucine into the system by monitoring the (1 0 0) reflection using synchrotron radiation. With respect to the systems discussed herein, Koolman and Rousseau investigated the addition of small amounts of l-leucine and l-valine to l-isoleucine crystallizations and related the effects of these impurities on the morphology and size of the isoleucine to possible substitution mechanisms in the crystal structure.[41] It was also shown via powder X-ray diffraction (PXRD) and HPLC methods that solid solutions of L-valine, l-isoleucine, and l-leucine can be formed although limited structural data were provided where the crystal structures of the solid solutions were assumed to be the same as those of the pure amino acids.[42] Very recently, a further study of L-isoleucine and L-valine solid solutions by Isakov et al. has detailed the phase behavior of this system in water and identified a new crystal structure associated with this complex.[43] Again, chromatographic and diffraction techniques were used to identify the species involved.

Herein we report a rapid and reproducible continuous antisolvent crystallization method to prepare solid solutions of hydrophobic amino acids: L-valine, L-leucine, and L-isoleucine (Scheme 1). Furthermore, we have identified new crystal structures of L-leucine/L-isoleucine and L-leucine/L-valine as well as confirming the recent report of a new form of L-isoleucine/L-valine.

Scheme 1. Molecular Form of (a) L-Leucine, (b) L-Isoleucine, and (c) L-Valine

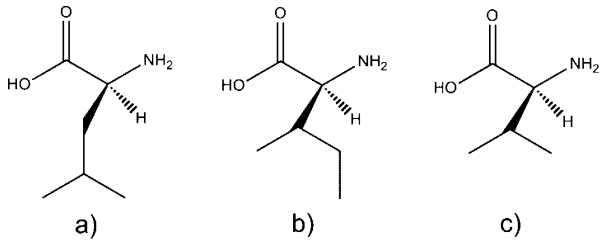

EXPERIMENTAL SECTION

Solid Solution Formation. Solid solutions of each pair of amino acids (≥98%, Sigma-Aldrich) were prepared using antisolvent crystallization on a 200 mL scale. An undersaturated aqueous solution was created by dissolving specific molar ratios of both amino acids in water (90:10, 70:30, 50:50, 30:70, and 10:90 molar ratio). For each pair of amino acids and defined composition, chilled antisolvent (isopropanol, Fisher Scientific) was added to the aqueous solution under agitation by a magnetic stirrer. The antisolvent was added all at once, resulting in a 95%w/w isopropanol solvent mixture. The resulting solid product was filtered and dried for analysis. The solid produced from these antisolvent crystallizations was used to determine the composition of the solid solutions and correlate it with the X-ray diffraction data.

Continuous Antisolvent Crystallization. For the continuous process, two different stoichiometric ratios were used to demonstrate the translation to a continuous antisolvent crystallization process. A process flow diagram of the continuous antisolvent crystallization process used here is shown in Figure 1. In this process, a preheated aqueous solution of amino acids at the required stoichiometric ratio (stream 1 at 45 °C) was continuously injected through a submerged stainless steel nozzle into the solution in the crystallizer vessel (V3) with a liquid volume of 50 mL. A flow rate (5 g/min) of stream 1 was delivered and controlled by an Ismatec external gear pumps (MCP-Z) with a magnetically coupled pump head (P1). The heat exchanger (E1) warmed the fluid and created a relative undersaturation of 0.4−0.5. Nozzles with two different internal diameters (0.2 and 0.6 mm) in connection with stream 1 flow rates generated different jet injection velocities (1.1−8.0 m/s) into the solution. Cold antisolvent isopropanol (stream 2 between 3.4 and 4.5 °C) with the flow rate of 95 g/min entered the crystallizer (V3) through Marprene tubing falling from the top of the vessel. The flow rates of stream 2 were delivered and controlled by a Watson-Marlow 520S peristaltic pump (P2) so that a constant mixing ratio of the two inlet streams 1 and 2 was maintained. The resulting temperature in the crystallizer was kept constant throughout the process (20 °C). This was achieved by balancing temperatures of colder inlet streams with an external jacket operating at a higher temperature (55 °C). Since the mean residence time in the crystallizer was very short, there was a significant temperature difference between the solution in the crystallizer and the vessel wall heated by the jacket. The reason for this was to minimize supersaturation at the vessel walls in order to decrease a propensity for fouling which would interfere with extended operation of the crystallizer in a continuous mode. Fouling was further prevented by immersing the crystallizer vessel in an ultrasonic bath (40 kHz, 50 W), which was operated while the continuous crystallization was running. The mean residence time in the crystallizer was 30 s, and the outlet stream was continuously withdrawn to a storage vessel where it was collected before subsequent filtration and drying. After relatively short transition times (up to 20 min), steady state operation of the crystallizer was achieved, where a crystal slurry was present in the crystallizer, and solid mass and crystallinity were not changing with time anymore during the subsequent steady state operation. Thus, a consistent quality of the solid phase product was achieved under steady state conditions in the continuous operating mode. The percentage yield for each compound can be found in Figure 2.

X-ray Diffraction Analysis. *Single Crystal X-ray Diffraction Analysis.* A number of crystallizations have been performed to crystallize the novel complexes. Initially equimolar quantities of two amino acids (~0.05 g, 0.4 mmol) were placed in a vial together with water (5 mL), and heat was applied in order to complete dissolution. After a period of a week at 25 °C, colorless crystals of sufficient quality for single crystal diffraction appeared through evaporative crystallization. Many crystallizations with varying ratios of components, including saturated solutions of the components, were used. All these crystallizations appeared to yield crystals of the same stoichiometry

DOI: 10.1021/acs.cgd.7b01105
Cryst. Growth Des. 2018, 18, 210−218

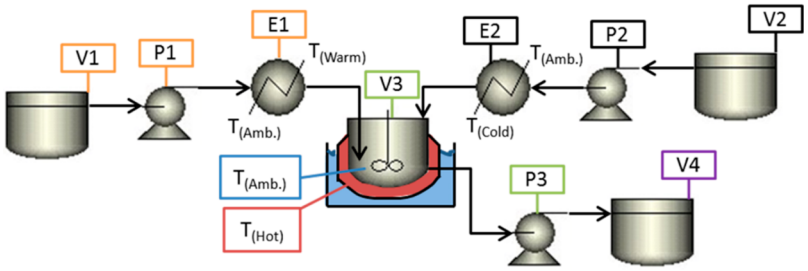

Figure 1. Continuous crystallization system setup. An undersaturated aqueous solutions of amino acids was fed from the feed vessel (V1) through the pump (P1) into the heat exchanger (E1) to heat to 45 °C before entering the crystallizer vessel (V3). Feed solution of isopropanol was fed through E2 to cool to 3.4−4.5 °C before entering V3. The slurry of crystals was extracted from V3 by a pump (P3) into the collection vessel (V4).

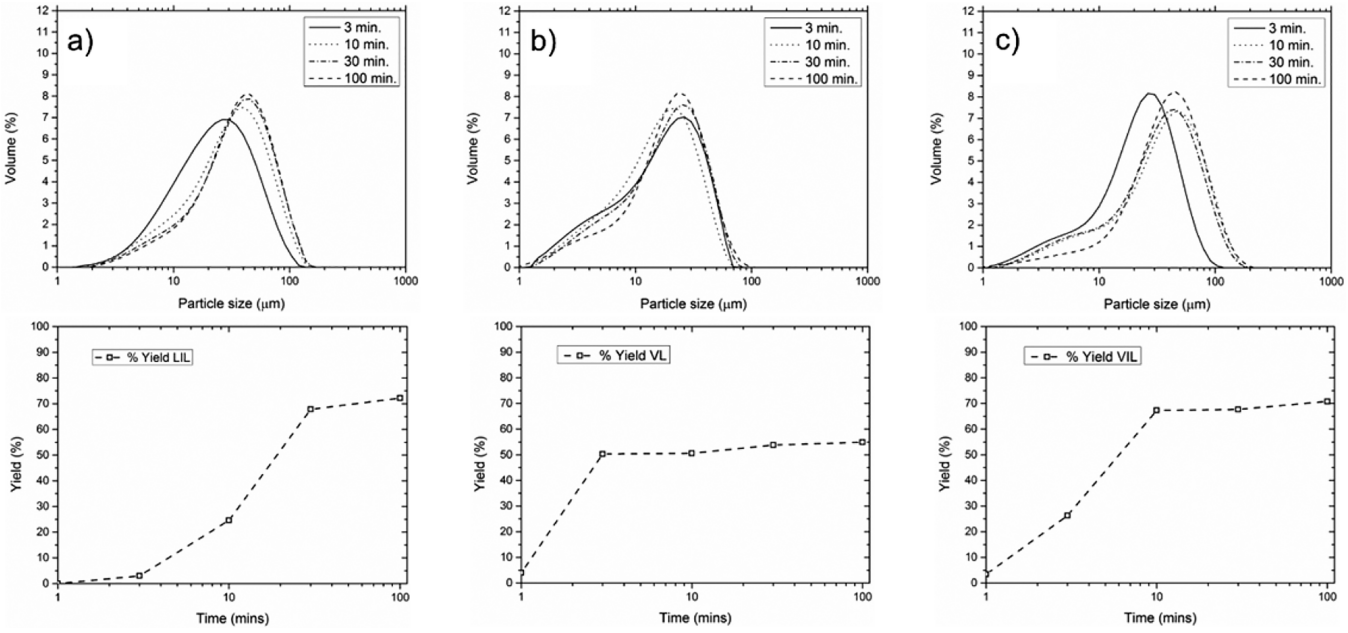

Figure 2. Particle size distribution for compound (a) **1**, (b) **2**, and (c) **3** over time (top) using laser diffraction and yields from the continuous process (50:50 molar ratio, bottom).

except for compound **2** where one crystal (identified using the UK National Crystallography Service) showed a different composition to that observed in our home laboratory. The details of the crystal structure analysis can be found in the Supporting Information.

Crystal Structure Determination. X-ray diffraction intensities for L-leucine/L-isoleucine (**1**), L-leucine/L-valine (**2NCS**), L-isoleucine/L-valine (**3**) were collected at I19 at Diamond Light Source (**1**)[44] and by the National Crystallography service (**2NCS** and **3**).[45] X-ray diffraction intensities for **2** were collected with Mo−Kα radiation on a Bruker KAPPA Apex II CCD diffractometer equipped with an Oxford Cryosystems Cryostream-*Plus* variable-temperature device operating at −150 °C.[46] Absorption corrections were carried out using the multiscan procedure *SADABS* (Sheldrick, 2004, based on the procedure described by Blessing, 1995).[47,48] The structures were solved by direct methods (SIR-92)[49] and refined by full-matrix least-squares against F ($I > 3\sigma$) using all data (CRYSTALS).[50] Because of the wavelength of the source (0.71073 Å), the chirality of the amino acids was assumed to be as stated by the manufacturer; however the molecules were consistent with each other in the model; i.e., both molecules were in the L-enantiomer.

The basic amino acid backbone (COO−C−N) and the first carbon of the chain were easily observed and used as the basic starting model for the refinements. From the difference map, extra peaks were observed that were of the correct geometry to be assigned to be the components of a specific amino acid. Once the two molecules were identified, further difference maps were used to find subsequent atoms that could only be assigned to a second component. These different components were assigned part numbers. The bond distances of the carbon side-chains (for compounds **1** and **2**) were restrained to be similar to those found in the Cambridge Structural Database[29] (1.54 Å for bonds between secondary carbons and 1.51 Å for bonds to primary carbons). Thermal similarity and vibrational restraints were also applied. The parts were given values of 50% occupancy and allowed to refine. **1** and **2** gave occupancy values that differed slightly, and the values quoted in the manuscript are average values with a standard deviation. **3** was more straightforward with the refinement remaining at 50% for one of the molecules in the asymmetric unit. In this case once the occupancy was established, the parts were not competitively refined. All hydrogen atoms attached to carbon atoms were geometrically placed, and those participating in hydrogen bonding, i.e., hydroxyl hydrogens, were found in the difference map. All non-H atoms were modeled with anisotropic displacement parameters.

Additional programs used included Materials Mercury 2.4,[51] PLATON as incorporated in WINGX.[52,53] Mercury, ChemBioDraw 12.0, OriginPro 9.0, and Vesta were used in the production of the figures.

Phase Analysis: Powder X-ray Diffraction. Laboratory Powder Diffraction. A small quantity (1−50 mg) of each sample from the antisolvent process was analyzed using PXRD data collected on a Bruker AXS D2-Phaser equipped with primary monochromated radiation (Cu−Kα_1 λ = 1.54056 Å; 30 kV and 10 mA), a LYNXEYE scintillation counter and rotating sample mount. Samples were ground lightly before being mounted on a six-position sample holder. Data

DOI: 10.1021/acs.cgd.7b01105
Cryst. Growth Des. 2018, 18, 210−218

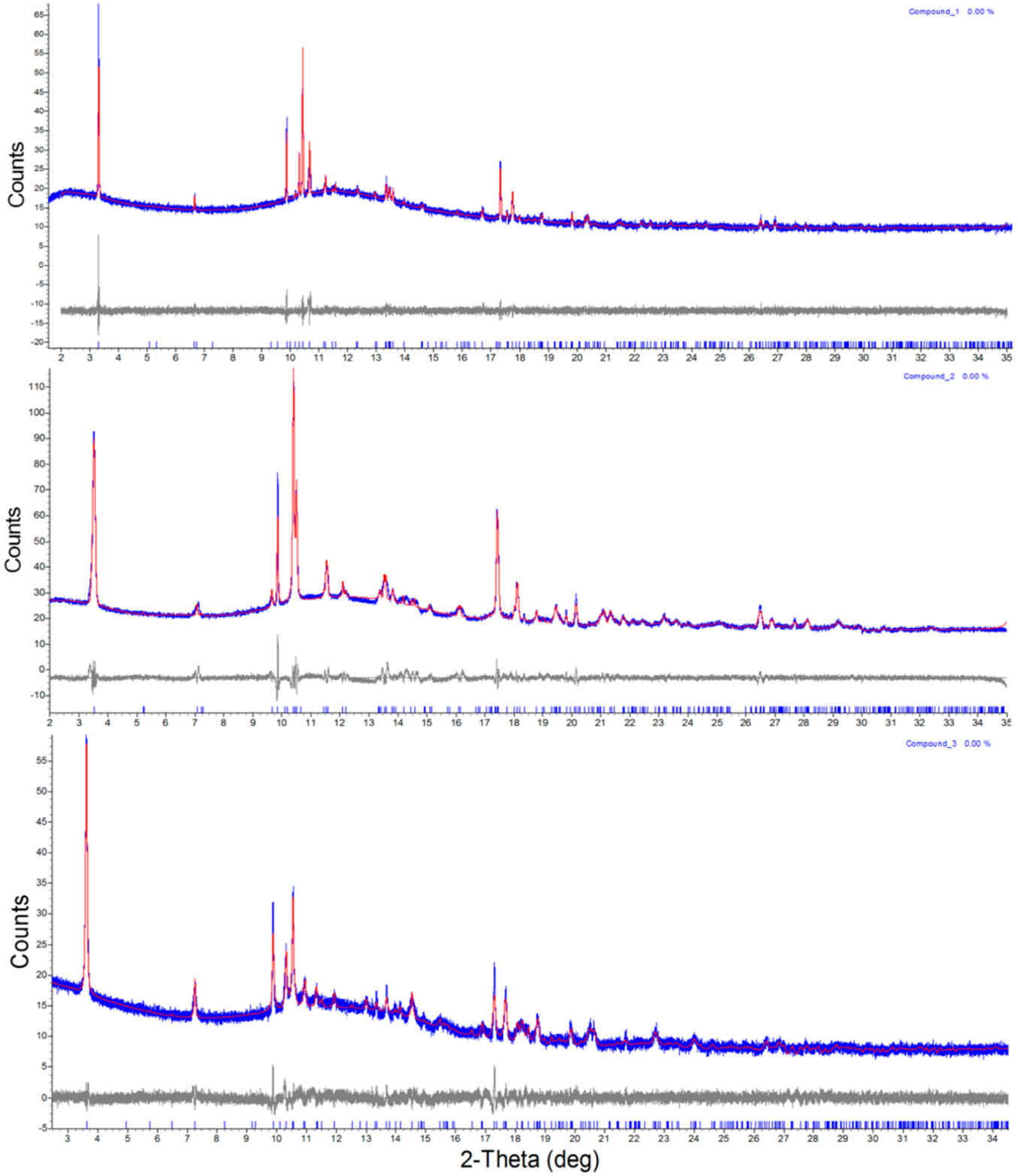

Figure 3. Pawley fits of the diffraction data from I11 for compounds **1** (top), **2** (middle), and **3** (bottom) obtained from continuous process (50:50 molar ratio) using the unit cell parameters from our single crystal work. The *d*-spacings correlate well with a 50% content of each component for each compound calculated from the batch experiments.

were collected from each sample in the range 4−35° 2θ with a 0.01° 2θ step size and 1 s step^{-1} count time.

Synchrotron Powder X-ray Diffraction. PXRD data were collected at −150 °C for the powder produced from the initial equimolar (50:50) antisolvent crystallization for compounds **1**, **2**, and **3** using Beamline I11 (HRPD) at the Diamond Light Source, Didcot, UK (λ = 0.826136(2) Å).[54,55] Samples were densely packed into 0.7 mm diameter thin-walled glass capillaries.

HPLC. HPLC with mass spectrometric detection was used to analyze the composition of the complexes from the batch antisolvent crystallization where the initial feedstock compositions were varied. Stock solutions of each amino acid were prepared by dissolving

DOI: 10.1021/acs.cgd.7b01105
Cryst. Growth Des. 2018, 18, 210−218

suitable amounts in HPLC grade water (Waters Milli-Q). (Note: 2% v/v acetonitrile was added to each amino acid solution prior to making to volume to aid dissolution.) Mixed working standards of the two required amino acids were prepared by diluting the stock solution with 80:20 acetonitrile/water such that the concentrations were in the range ~1−10 or 1−12 μg/mL. Two chromatographic systems were used for the analysis. Compounds **1** and **2** were analyzed using an isocratic HPLC system. This system consisted of an Agilent 1260 infinity HPLC (Agilent Technologies LDA UK Limited, Stockport, Cheshire, UK). The mobile phase was 20% 50 mM ammonium formate in water and 80% acetonitrile at a flow rate of 500 μL/min. A SeQuant ZIC-HILIC column (HiChrom, Theale, Berkshire) was used (150 × 4.6 mm, 5 μm particle size) at a temperature of 30 °C. The injection volume was 10 μL. Detection of the amino acids was achieved using an Agilent 6460 Triple Quad mass spectrometer (Agilent Technologies LDA UK Limited, Stockport, Cheshire, UK) equipped with an electrospray source. The electrospray needle was maintained at 2.5 kV. The gas temperature was 300 °C. Nebulizing gas and sheath gas flows were at 3 L/min and 4 L/min, respectively. The mass spectrometer was operated under MRM mode with the fragmentor set at 135 and the collision energy set at 20. The mass transitions (precursor → product) monitored were m/z 132 → 86 for leucine and isoleucine and 118 → 72 for valine. The approximate retention times were 9.4 min (leucine), 10.0 min (isoleucine), and 12.5 min (valine). Valine was well resolved (Rs > 4) from the other two components, and leucine and isoleucine also showed acceptable resolution (Rs = 1.56).

For compound **3** a gradient HPLC method was used for the analysis. This system consisted of a Thermo Finnigan Surveyor HPLC (ThermoFisher Scientific, Altrincham, Cheshire, UK). The mobile phases for HPLC were (A) 20 mM ammonium carbonate in water and (B) acetonitrile. Gradient runs were programmed using a linear gradient from 20% B to 50% B over 30 min at a flow of 300 μL/min. The equilibration time of the column between injections was 8 min. A SeQuant ZIC-pHILIC column (HiChrom, Theale, Berkshire) was used (150 × 4.6 mm, 5 μm particle size) at ambient temperature (approximately 20 °C). The injection volume was 2 μL. Detection of the amino acids was achieved using a Finnegan LTQ Orbitrap Fourier-Transform mass spectrometer (ThermoFisher Scientific, Altrincham, Cheshire, UK) equipped with an electrospray source. The electrospray needle was maintained at 4.5 kV and 275 °C. Sheath and auxiliary gas flows were set at 50 and 15 respectively. A full mass scan was performed in positive ion mode with a mass range of m/z 100−1200, and the resolution was 30000. Extracted ions at m/z 118.09 (valine) and m/z 132.1 isoleucine) were used for quantification purposes. The approximate retention times were 9.7 min (isoleucine) and 11.1 min (valine). Valine and isoleucine were baseline resolved (Rs > 2). Typical calibration lines used in the sample analysis can be found in Table ES2. Recoveries were confirmed using separately prepared standard solutions.

Particle Size Distribution. A Malvern Mastersizer (APA2000, Malvern Instruments Ltd., UK) laser diffraction instrument was used to determine the particle size distribution of solid powder samples. The instrument was conditioned with mother-liquor from the crystallization experiment to account for background scattering. The sample crystal slurries from the crystallizer outlet tube were pipetted into the Mastersizer sample container unit until the instrument indicated that the optimum solid concentration had been achieved for a measurement. The refractive index of 1.65 was used for the measurement and data analysis.

RESULTS AND DISCUSSION

Identification of the Solid Solution. Previous work by Kurosawa et al.[42] and Isakov et al.[43] has shown that the three amino acids, L-leucine, L-isoleucine, and L-valine, formed solid solutions via the interpretation of the (0 0 1) reflection from the PXRD patterns and HPLC methods. One of the limitations of the Kurosawa paper was that they assumed that the crystal structure of the materials remained the same at each composition. This was rectified for the isoleucine/valine system where Isakov and co-workers identified a new crystal form, a C-

Table 1. Crystal Solid Yield at Various Experimental Runtimes

	solid yield [%]		
time [min]	1	2	3
1	0.0	4.0	3.4
3	3.0	50.3	26.3
10	24.6	50.6	67.3
30	67.8	53.8	67.7
100	72.2	54.9	70.8

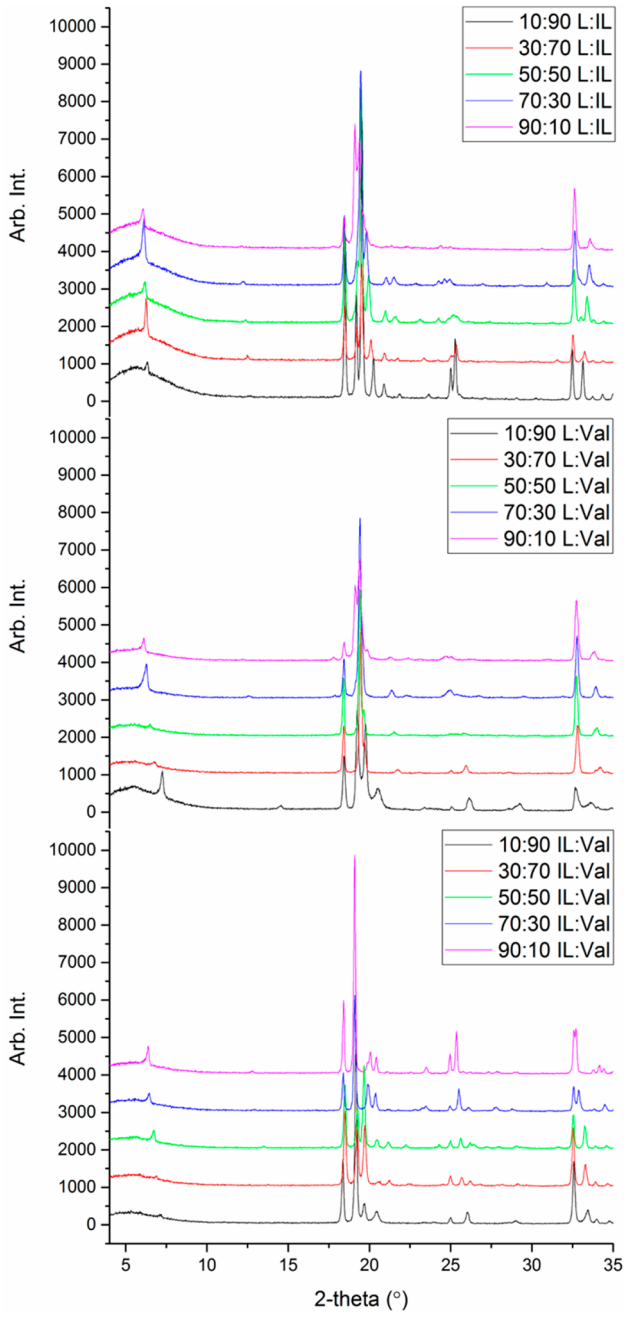

Figure 4. Waterfall plots of the three compounds with varying molar ratio composition (refer to Table 2 for exact composition identified in HPLC). The change in the peak positions indicating the slow change in the unit cell parameters with addition of a second component.

DOI: 10.1021/acs.cgd.7b01105
Cryst. Growth Des. 2018, 18, 210−218

Table 2. Position of the (0 0 1) Reflection ((2 0 0) for Compound 3) for Each Compound, Obtained from Pawley Fits to the Room Temperature Data, with Respect to the Concentration of the Reactants[a]

compound **1** leucine % content (mass spec.)	*d*-spacing observed	structure	*d*-spacing of Kurosawa et al. with % leucine/ isoleucine
0	13.94[41]	IL	
10.12	13.98	SS	14.24 (14%)
31.40	14.16	SS	14.48 (34%)
51.15	14.29	SS	14.52 (46%)
68.67	14.39	SS	14.56 (60%)
92.05	14.55	SS	14.80 (91%)
100	14.62[60]	L	
compound **2** leucine % content (mass spec.)	*d*-spacing observed	structure	*d*-spacing of Kurosawa et al. with % leucine/ isoleucine
0	12.06[61]	V	
7.43	12.15	V	12.50 (13%)
34.04	13.03	SS	13.04 (28%)
52.06	13.47	SS	13.37 (45%)
74.34	14.04	SS	14.32 (77%)
94.14	14.41	SS	14.56 (92%)
100	14.62[60]	L	
compound **3** hypothetical isoleucine % content	*d*-spacing observed	structure	*d*-spacing of Kurosawa et al. with % leucine/ isoleucine
0	12.06[61]	V	
10.90	12.35	V	12.36 (11%)
35.59	12.83	SS	12.80 (28%)
51.50	13.08	SS	13.23 (58%)
75.87	13.62	SS	13.34 (89%)
75.87	14.08	IL	13.99 (89%)
87.56	13.80	SS	13.26 (95%)
87.56	14.03	IL	14.01 (95%)
100	13.94[41]	IL	

[a]The crystal structure that was used to fit the data are presented alongside the results of Kurosawa et al. The values in parentheses are the percentage of leucine or isoleucine corresponding to their X-ray data.

centered cell related to the basic amino acid unit cells. At the same time, through small scale batch evaporative crystallizations, we have been able to isolate crystals of the solid solutions of leucine/isoleucine (**1**), leucine/valine (**2**), and isoleucine/valine (**3**) with unit cell lengths close to the original phases but with a different β-angle. The structures were initially elucidated using single crystal X-ray diffraction using data collected by the National Crystallography Service (NCS)[45] and Diamond Light Source Rapid Access Service (RAS) at beamline I19.[56] After a period of two months in solution, the crystal quality improved through annealing processes such that in-house data could be used to help verify the quantities of each component and confirm the NCS and RAS data. The proportion of each constituent is not stoichiometric, and therefore five data sets were collected for each sample in order to be sure of the proportion of each amino acid within the crystals in each batch. The percentage composition in **1** is 59(2)% isoleucine, **2** is 61(3)% leucine, and **3** is 75% valine. The composition of the latter did not show any variation between data sets and was fixed hence no error. Interestingly, for **2**, the extent of this disorder altered slightly over time. Analysis of small less mature crystals using NCS showed that the percentage occupancy for **2** was 73:27 leucine/valine cf. 61:39 from more mature crystals, indicating the change in the composition of the solution.

The unit cells of all three solid solutions are different from their parent compounds with a significant change in the β-angle of the cell for compounds **1** and **2**, and there is an addition of C-centring in compound **3**, so while the unit cell dimensions are similar the packing of the molecules has been altered by the addition of a second component in line with the observations of Isakov et al. These observations are contrary to the assumptions made by Kurosawa et al. that the crystal structure was the same as the pure phases; nevertheless we do observe the non-stoichiometric quantities of materials indicating the solid solution have been formed. Compounds **1** (Figure ESI) and **2** crystallize in $P2_1$, while compound **3** crystallizes in $C2$ with all forms possessing two molecules in the asymmetric unit. The basic amino acid hydrogen bonded chains exist in all three complexes and have a consistent geometry compared with the hydrogen bonding observed in the pure amino acid structures; i.e., the disorder that has arisen due to the cocrystallization process has not affected these stronger intermolecular interactions.[57−59] The overall structure of the materials remains as a bilayer where head groups interact via hydrogen bonding with those of neighboring chains and the hydrophobic tail groups of the amino acids interact with those of a different chain. The crystallographic information can be found in the Supporting Information.

Antisolvent Crystallization. Having established that the solid solutions of the three compounds crystallized in different crystal structures, we investigated the ability of continuous antisolvent preparative routes to form these complex systems. The flexibility of the continuous approach is ideal for the production of these solid solution phases; the short residence times means that the composition of the resulting solid solution can be varied and tuned rapidly. This method was chosen as established synthetic routes; e.g., ball-milling, liquid-assisted grinding, and slurry methods, failed to produce pure products.

Starting with two different molar ratios of the two components, 50:50 and 40:60, in the inlet stream 1, we used the continuous antisolvent approach to produce gram quantities. The analysis using PXRD (Diamond Light Source, Figure 3), particle size distribution and yield present here were performed on the 50:50 ratio. The mean residence time in the crystallizer was 30 s where the product was continuously withdrawn to a storage vessel. After approximately 20 min, steady state operation of the crystallizer was achieved, where a slurry was present in the crystallizer and particle size distribution was not changing with time (Figure 2). Thus, a consistent quality of the product was achieved under steady state conditions in the continuous operating mode. The continuous process provided steady-state yields (based on the total amount of amino acids in the inlet feed) of 70% for **1**, 50% for **2**, and 70% for **3** were observed after experimental running times of 20, 3, and 10 min, respectively (Table 1 and Figure 2). These yields can be further improved by varying the solvent to antisolvent ratio. Figure 2 shows the particle size distributions for the crystals produced in the crystallizer (rather that the storage vessel) where the time indicated represents the runtime of the experiment. One can observe the reduction in the number of smaller crystallites during the continuous process such that by 10 min a steady particle size was being produced with a small portion of crystallites with smaller dimensions. The particle sizes showed an asymmetric distribution skewed to

DOI: 10.1021/acs.cgd.7b01105
Cryst. Growth Des. 2018, 18, 210−218

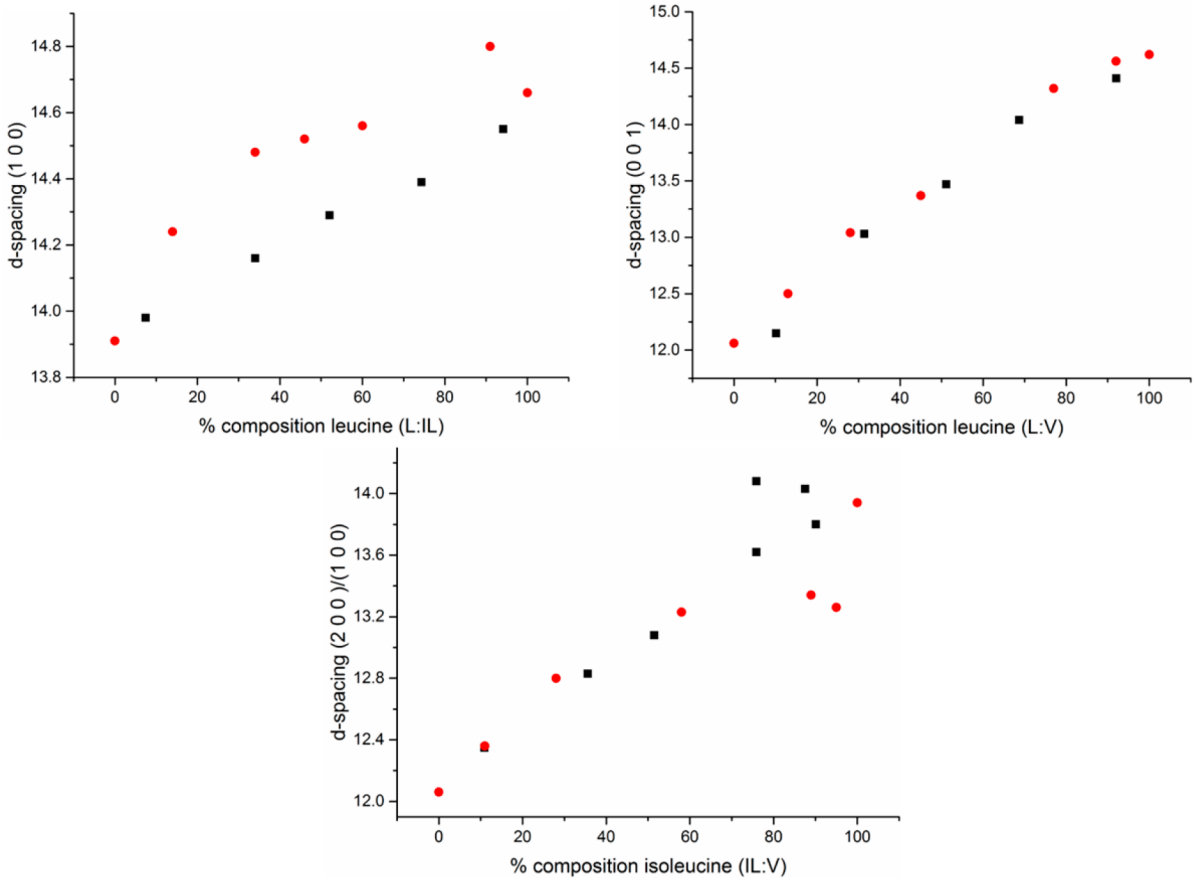

Figure 5. Plots of the (1 0 0) or (2 0 0) reflection vs % composition observed for our data (black squares) and that of Kurosawa (red circles).[42]

smaller sizes with a mode being around 40, 25, 50 μm for **1**, **2**, and **3**, respectively.

Identification of Solid Phase from Continuous Process. The solids produced from the continuous antisolvent crystallization (50:50 ratio) were analyzed via PXRD and Pawley fitted against the known phases including the new structures identified in this paper. Figure 3 shows a Pawley fit of the PXRD data collected at I11, Diamond Light Source (−150 °C; λ = 0.826939 Å) using cell parameters of the novel phases **1**−**3**. These data are collected at −150 °C and therefore show a slight shift with respect to the results of Kurosawa et al.[42] and Isakov et al.[43] There are a number of tick marks between 2θ values of 4−8° which have near zero intensity, which is representative of the structure.

Correlation of Solid Solution Composition and X-ray Diffraction Data. A more extensive analysis of the solid solutions was performed using products from the batch antisolvent experiments to correlate the PXRD pattern to the solid solution composition so that a comparison with the methodologies in the literature could be performed (Figure 4). Table 2 shows the proportions of each component (as identified by HPLC) as a function of the *d*-spacing observed (20 °C) and the type of structure that fits the data, e.g., pure components or solid solution. These data are also compared with those of Kurosawa in which we have used data for the samples of similar composition. The HPLC was performed without modification of the amino acids unlike previous work where the amino acids were subject to prederivatization using *o*-phthaldialdehyde; we have avoided this step by using the ZIC-HILIC column that allows clear separation of the amino acids, even leucine and isoleucine.

For compound **1** we observe that the solid solution phase can be fit to all our data at various compositions. It is clear that our data and that of Kurosawa et al.[42] are substantially different from one another with ours showing a much more linear change with composition (Figure 5). Both studies observe only one peak, which suggests that the phases that were produced were pure. This reflects the subtle differences in the molecular structure of the two components. Isoleucine and leucine are the same size of molecule with a difference in the connectivity of the tail group. Substitution of isoleucine into the leucine structure has caused a change in the unit cell parameters mainly in the β-angle 104° cf. 94.06°.[60]

The diffraction and composition data for compound **2** from our study fits well with previous work showing a linear change of the *d*-spacing with the composition of the solid; however at 10% leucine the structure reverts to the valine structure as identified by the unit cell parameters. Again there is a shift in the β-angle to 109° from ∼94° and 90° for leucine and valine unit cell parameters, respectively.

Compound **3** shows some indication that toward 100% composition of isoleucine there is a mixed phase with the solid solution and the pure isoleucine solids; this is in line with the observations of Isakov et al.[43] The HPLC reveals that our composition is a reasonably good fit to the ideal values, i.e., 10, 30, 50, 70, and 90%. We also observe a biphasic nature down to 75% isoleucine with the second phase fitting the unit cell parameters of pure isoleucine Form I. Our data for compound **3** follows that of Kurosawa[42] until there is a greater quantity of

DOI: 10.1021/acs.cgd.7b01105
Cryst. Growth Des. 2018, 18, 210−218

isoleucine (89 and 95%). At this point their data fall away from the projected movement, while our data remain in line with what one would suspect for a solid solution. In terms of the composition of the solid we have identified it is a 3:1 valine/isoleucine (75%) solid solution which is at the extremity of the V_2I phase that Isakov highlighted in their study; however interestingly the unit cell is larger in our case (both studies were collected at −173 °C), which is counterintuitive given there is a greater portion of the smaller constituent. The packing is similar, bearing in mind the discrepancy of chirality from the structure in the CSD (ALIHUA), with no particular features that are different to guide any reasonable argument as to the differences. The previous determination has both molecules substituted with isoleucine contrary to our determination but despite this the *a*-axis (where the tails group interact) is longer.

One methodological note to make, that may impact our results compared with that of Isakov et al.,[43] is that the resulting solid from our experiment was harvested from solution and was not ever subject to complete evaporation unlike the previous study; hence the solubility of the initial components during the antisolvent crystallization will have an impact on the resulting solid collected. The solubility of the solid solution was shown by Isakov to be higher than the isoleucine solubility, hence the reason that we observe the mixed phase in the solid.

CONCLUSIONS

This study has shown that we are able to control the formation of tunable solid solutions of hydrophobic amino acids using a novel antisolvent crystallization approach. We have also shown that solid solutions can be formed easily and rapidly through continuous antisolvent crystallization. The continuous process is rapid, since the mean residence time in the crystallizer is only 30 s, and it can run at steady state over extended periods of time, offering considerable advantages over traditional batch based scale up approaches. In high value chemicals manufacturing, reproducibility is a key attribute and can be achieved through continuous operation at steady state. The development, testing, and implementation of continuous crystallization approaches are of particular importance in light of increased interest in continuous manufacturing processes for pharmaceuticals, and other high value chemical products can be formed routinely using continuous antisolvent crystallization.

ASSOCIATED CONTENT

Supporting Information

The Supporting Information is available free of charge on the ACS Publications website at DOI: 10.1021/acs.cgd.7b01105

Table ES1. Crystallographic information for **1**, **2**, and **3**. Figure ES1. Images of single crystals from the slow evaporation route used in the determination of the structure from single-crystal diffraction. Figure ES2. Calibration graphs used for the determination of the composition of compounds **1** and **2**. Figure ES3. Calibration graphs used for the determination of the composition of compound **3**. Table ES2. Results of the HILIC HPLC analysis of the products of the antisolvent crystallization (PDF)

.

Accession Codes

CCDC 997468−997471 (structures **1**, **2**, **2NCS**, and **3**) contain the supplementary crystallographic data for this paper. These data can be obtained free of charge via www.ccdc.cam.ac.uk/data_request/cif, or by emailing data_request@ccdc.cam.ac.uk, or by contacting The Cambridge Crystallographic Data Centre, 12 Union Road, Cambridge CB2 1EZ, UK; fax: +44 1223 336033.

AUTHOR INFORMATION

Corresponding Authors

*(A.J.F.) Fax: +44-(0)-141-552- 2562; tel: +44 (0)141 548 4877; e-mail: alastair.florence@strath.ac.uk.
*(J.S.) E-mail: jan.sefcik@strath.ac.uk.
*(I.D.H.O.) Fax: +44-(0)-141-552- 2562; Tel: +44-(0)-141-548-2157; E-mail: iain.oswald@strath.ac.uk.

ORCID

Vaclav Svoboda: 0000-0002-2386-7112
Alastair J. Florence: 0000-0002-9706-8364
Iain D. H. Oswald: 0000-0003-4339-9392

Notes

The authors declare no competing financial interest.
All data underpinning this publication are openly available from the University of Strathclyde KnowledgeBase at http://doi.org/10.15129/5713a62d-2fa6-4a71-9a18-d1373cbf409e.

ACKNOWLEDGMENTS

We thank the EPSRC UK National Crystallography Service at the University of Southampton and Sarah Barnett of I19 Diamond Light Source Rapid Access Service for the collection of the crystallographic data. We thank the EPSRC CIM in Continuous Manufacturing and Crystallization (EP/I033459/1), the EPSRC DTC in Continuous Manufacturing and Crystallization (EP/K503289/1) for funding as well as fellowship for IDHO (EP/N015401/1). We also thank the University of Punjab (SAR), Scottish Funding Council Horizon SPIRIT studentship (US), for funding.

REFERENCES

(1) Bond, A. D. *CrystEngComm* **2007**, *9*, 833−834.
(2) Aitipamula, S.; Banerjee, R.; Bansal, A. K.; Biradha, K.; Cheney, M. L.; Choudhury, A. R.; Desiraju, G. R.; Dikundwar, A. G.; Dubey, R.; Duggirala, N.; Ghogale, P. P.; Ghosh, S.; Goswami, P. K.; Goud, N. R.; Jetti, R. K. R.; Karpinski, P.; Kaushik, P.; Kumar, D.; Kumar, V.; Moulton, B.; Mukherjee, A.; Mukherjee, G.; Myerson, A. S.; Puri, V.; Ramanan, A.; Rajamannar, T.; Reddy, C. M.; Rodriguez-Hornedo, N.; Rogers, R. D.; Row, T. N. G.; Sanphui, P.; Shan, N.; Shete, G.; Singh, A.; Sun, C. Q. C.; Swift, J. A.; Thaimattam, R.; Thakur, T. S.; Thaper, R. K.; Thomas, S. P.; Tothadi, S.; Vangala, V. R.; Vishweshwar, P.; Weyna, D. R.; Zaworotko, M. J. *Cryst. Growth Des.* **2012**, *12*, 4290−4291.
(3) *Pharmaceutical Salts and Co-Crystals*; Royal Society of Chemistry, 2011.
(4) Center for Drug Evaluation and Research, Guidance for Industry Regulatory Classification of Pharmaceutical Co-Crystals. U.S. Department of Health and Human Services; Food and Drug Administration, 2013.
(5) Center for Drug Evaluation and Research, Regulatory Classification of Pharmaceutical Co-Crystals Guidance for Industry. U.S. Department of Health and Human Services; Food and Drug Administration, 2016.
(6) Yan, D.; Evans, D. G. *Mater. Horiz.* **2014**, *1*, 46−57.
(7) Yan, D. P.; Delori, A.; Lloyd, G. O.; Friscic, T.; Day, G. M.; Jones, W.; Lu, J.; Wei, M.; Evans, D. G.; Duan, X. *Angew. Chem., Int. Ed.* **2011**, *50*, 12483−12486.
(8) Bolton, O.; Simke, L. R.; Pagoria, P. F.; Matzger, A. J. *Cryst. Growth Des.* **2012**, *12*, 4311−4314.

DOI: 10.1021/acs.cgd.7b01105
Cryst. Growth Des. 2018, 18, 210−218

(9) McNamara, D. P.; Childs, S. L.; Giordano, J.; Iarriccio, A.; Cassidy, J.; Shet, M. S.; Mannion, R.; O'Donnell, E.; Park, A. *Pharm. Res.* **2006**, *23*, 1888−1897.
(10) Trask, A. V.; Motherwell, W. D. S.; Jones, W. *Cryst. Growth Des.* **2005**, *5*, 1013−1021.
(11) Trask, A. V.; Motherwell, W. D. S.; Jones, W. *Int. J. Pharm.* **2006**, *320*, 114−123.
(12) Delori, A.; Maclure, P.; Bhardwaj, R. M.; Johnston, A.; Florence, A. J.; Sutcliffe, O.; Oswald, I. D. H. *CrystEngComm* **2014**, *16*, 5827.
(13) Wang, J. R.; Zhou, C.; Yu, X. P.; Mei, X. F. *Chem. Commun.* **2014**, *50*, 855−858.
(14) Childs, S. L.; Kandi, P.; Lingireddy, S. R. *Mol. Pharmaceutics* **2013**, *10*, 3112−3127.
(15) Gagniere, E.; Mangin, D.; Puel, F.; Bebon, C.; Klein, J. P.; Monnier, O.; Garcia, E. *Cryst. Growth Des.* **2009**, *9*, 3376−3383.
(16) Gagniere, E.; Mangin, D.; Puel, F.; Rivoire, A.; Monnier, O.; Garcia, E.; Klein, J. R. *J. Cryst. Growth* **2009**, *311*, 2689−2695.
(17) Dhumal, R. S.; Kelly, A. L.; York, P.; Coates, P. D.; Paradkar, A. *Pharm. Res.* **2010**, *27*, 2725−2733.
(18) Padrela, L.; Rodrigues, M. A.; Velaga, S. R.; Matos, H. A.; de Azevedo, E. G. *Eur. J. Pharm. Sci.* **2009**, *38*, 9−17.
(19) Ross, S. A.; Lamprou, D. A.; Douroumis, D. *Chem. Commun.* **2016**, *52*, 8772−8786.
(20) Zhao, L.; Raval, V.; Briggs, N.; Bhardwaj, R. M.; McGlone, T.; Oswald, I. D. H.; Florence, A. J. *CrystEngComm* **2014**, *16*, 5769.
(21) Svoboda, V.; MacFhionnghaile, P.; McGinty, J.; Connor, L. E.; Oswald, I. D. H.; Sefcik, J. *Cryst. Growth Des.* **2017**, *17*, 1902−1909.
(22) Dittrich, B.; Pfitzenreuter, S.; Hubschle, C. B. *Acta Crystallogr., Sect. A: Found. Crystallogr.* **2012**, *68*, 110−116.
(23) Funnell, N. P.; Dawson, A.; Marshall, W. G.; Parsons, S. *CrystEngComm* **2013**, *15*, 1047−1060.
(24) Johnstone, R. D. L.; Francis, D.; Lennie, A. R.; Marshall, W. G.; Moggach, S. A.; Parsons, S.; Pidcock, E.; Warren, J. E. *CrystEngComm* **2008**, *10*, 1758−1769.
(25) Abagaro, B. T. O.; Freire, P. T. C.; Silva, J. G.; Melo, F. E. A.; Lima, J. A.; Filho, J. M.; Pizani, P. S. *Vib. Spectrosc.* **2013**, *66*, 119−122.
(26) Minkov, V. S.; Boldyreva, E. V.; Drebushchak, T. N.; Gorbitz, C. H. *CrystEngComm* **2012**, *14*, 5943−5954.
(27) Paukov, I. E.; Kovalevskaya, Y. A.; Boldyreva, E. V. *J. Therm. Anal. Calorim.* **2013**, *111*, 2059−2062.
(28) Trabattoni, S.; Moret, M.; Campione, M.; Raimondo, L.; Sassella, A. *Cryst. Growth Des.* **2013**, *13*, 4268−4278.
(29) Allen, F. *Acta Crystallogr., Sect. B: Struct. Sci.* **2002**, *58*, 380−388.
(30) Gorbitz, C. H. *Crystallogr. Rev.* **2015**, *21*, 160−212.
(31) Gorbitz, C. H. *Acta Crystallogr., Sect. E: Struct. Rep. Online* **2004**, *60*, o626−o628.
(32) Soldatov, D. V.; Moudrakovski, I. L.; Grachev, E. V.; Ripmeester, J. A. *J. Am. Chem. Soc.* **2006**, *128*, 6737−6744.
(33) Gorbitz, C. H. *New J. Chem.* **2003**, *27*, 1789−1793.
(34) Dalhus, B.; Gorbitz, C. H. *Acta Crystallogr., Sect. B: Struct. Sci.* **2000**, *56*, 720−727.
(35) Dalhus, B.; Gorbitz, C. H. *Acta Crystallogr., Sect. C: Cryst. Struct. Commun.* **1999**, *55*, 1547−1555.
(36) Dalhus, B.; Gorbitz, C. H. *Acta Crystallogr., Sect. C: Cryst. Struct. Commun.* **1999**, *55*, 1105−1112.
(37) Dalhus, B.; Gorbitz, C. H. *Acta Crystallogr., Sect. B: Struct. Sci.* **1999**, *55*, 424−431.
(38) Fabian, L.; Chisholm, J. A.; Galek, P. T. A.; Motherwell, W. D. S.; Feeder, N. *Acta Crystallogr., Sect. B: Struct. Sci.* **2008**, *64*, 504−514.
(39) Kamei, T.; Hasegawa, K.; Kashiwagi, T.; Suzuki, E.; Yokota, M.; Doki, N.; Shimizu, K. *J. Chem. Eng. Data* **2008**, *53*, 2801−2806.
(40) Kamei, T.; Hasegawa, K.; Kashiwagi, T.; Suzuki, E.; Yokota, M.; Doki, N.; Shimizu, K. *J. Chem. Eng. Data* **2008**, *53*, 1338−1341.
(41) Koolman, H. C.; Rousseau, R. W. *AIChE J.* **1996**, *42*, 147−153.
(42) Kurosawa, H.; Teja, A. S.; Rousseau, R. W. *Fluid Phase Equilib.* **2005**, *228-229*, 83−87.
(43) Isakov, A. I.; Kotelnikova, E. N.; Muenzberg, S.; Bocharov, S. N.; Lorenz, H. *Cryst. Growth Des.* **2016**, *16*, 2653−2661.
(44) Collected via the I19 Rapid access service at Diamond Light Source (Project MT7150).
(45) Coles, S. J.; Gale, P. A. *Chem. Sci.* **2012**, *3*, 683−689.
(46) Cosier, J.; Glazer, A. M. *J. Appl. Crystallogr.* **1986**, *19*, 105−107.
(47) Sheldrick, G. M. *SADABS* Version 2004-1; Bruker-AXS: Madison, WI, 2004.
(48) Blessing, R. H. *Acta Crystallogr., Sect. A: Found. Crystallogr.* **1995**, *51*, 33−38.
(49) Altomare, A.; Cascarano, G.; Giacovazzo, C.; Guagliardi, A. *J. Appl. Crystallogr.* **1993**, *26*, 343−350.
(50) Betteridge, P. W.; Carruthers, J. R.; Cooper, R. I.; Prout, K.; Watkin, D. J. *J. Appl. Crystallogr.* **2003**, *36*, 1487−1487.
(51) Macrae, C. F.; Bruno, I. J.; Chisholm, J. A.; Edgington, P. R.; McCabe, P.; Pidcock, E.; Rodriguez-Monge, L.; Taylor, R.; van de Streek, J.; Wood, P. A. *J. Appl. Crystallogr.* **2008**, *41*, 466−470.
(52) Farrugia, L. J. *J. Appl. Crystallogr.* **2012**, *45*, 849−854.
(53) Spek, A. L. *J. Appl. Crystallogr.* **2003**, *36*, 7−13.
(54) Tang, C. C.; Thompson, S. P.; Hill, T. P.; Wilkin, G. R.; Wagner, U. H. *Z. Kristallogr.* **2007**, *2007*, 153−158.
(55) Thompson, S. P.; Parker, J. E.; Potter, J.; Hill, T. P.; Birt, A.; Cobb, T. M.; Yuan, F.; Tang, C. C. *Rev. Sci. Instrum.* **2009**, *80*, 075107.
(56) Nowell, H.; Barnett, S. A.; Christensen, K. E.; Teat, S. J.; Allan, D. R. *J. Synchrotron Radiat.* **2012**, *19*, 435−441.
(57) Gorbitz, C. H.; Dalhus, B. *Acta Crystallogr., Sect. C: Cryst. Struct. Commun.* **1996**, *52*, 1754−1756.
(58) Gorbitz, C. H.; Dalhus, B. *Acta Crystallogr., Sect. C: Cryst. Struct. Commun.* **1996**, *52*, 1464−1466.
(59) Dalhus, B.; Gorbitz, C. H. *Acta Chem. Scand.* **1996**, *50*, 544−548.
(60) Coll, M.; Solans, X.; Font-Altaba, M.; Subirana, J. A. *Acta Crystallogr., Sect. C: Cryst. Struct. Commun.* **1986**, *42*, 599−601.
(61) Torii, K.; Iitaka, Y. *Acta Crystallogr., Sect. B: Struct. Crystallogr. Cryst. Chem.* **1970**, *26*, 1317−1326.

DOI: 10.1021/acs.cgd.7b01105
Cryst. Growth Des. 2018, 18, 210−218